DEPARTMENT OF TRANSPORTATION

Mechanical Response of a Composite Steel, Concrete-Filled Pile

Joseph Labuz, Principal Investigator
Department of Civil, Environmental, and Geo- Engineering
University of Minnesota

June 2018

Research Project
Final Report 2018-20

To request this document in an alternative format, such as braille or large print, call 651-366-4718 or 1-800-657-3774 (Greater Minnesota) or email your request to ADArequest.dot@state.mn.us. Please request at least one week in advance.

Technical Report Documentation Page

1. Report No.	2.	3. Recipients Accession No.
MN/RC 2018-20		

4. Title and Subtitle	5. Report Date
Mechanical Response of a Composite Steel, Concrete-Filled Pile	June 2018
	6.
7. Author(s) Chen Hu, Jacob Sharpe, and Joseph Labuz	8. Performing Organization Report No.
9. Performing Organization Name and Address Department of Civil, Environmental, and Geo- Engineering University of Minnesota 500 Pillsbury Dr SE Minneapolis, MN 55455	10. Project/Task/Work Unit No. CTS#2015023 11. Contract (C) or Grant (G) No. (c) 99008 (wo) 165
12. Sponsoring Organization Name and Address Minnesota Department of Transportation Research Services & Library 395 John Ireland Boulevard, MS 330 St. Paul, Minnesota 55155-1899	13. Type of Report and Period Covered Final Report 14. Sponsoring Agency Code

15. Supplementary Notes

http://mndot.gov/research/reports/2018/201820.pdf

16. Abstract (Limit: 250 words)

A steel pipe-pile section, filled with concrete, was instrumented and tested under axial load. Two types of strain gages, resistive and vibrating wire, were mounted to the steel-pipe pile and checked by determining the known Young's modulus of steel E^s. The steel section was filled with concrete and a resistive embedment gage was placed in the concrete during the filling process to measure axial strain of the concrete. The axial load – axial strain responses of the steel (area A^s) and concrete (area A^c) were evaluated. The stiffening of concrete, related to curing, was also studied.

Assuming the boundary condition of uniform axial displacement, *i.e.*, equal axial strain in the steel and concrete, $\varepsilon_z^s = \varepsilon_z^c = \varepsilon_z$, the sum of the forces carried by the two materials, $F^s + F^c$, where $F^s = \varepsilon_z * E^s * A^s$ and $F^c = \varepsilon_z * E^c * A^c$, provides a reasonable estimate – within 3% – of the pile force. For the particular specimen studied (12 in. ID, 0.25 in. wall thickness), the stiffness of the composite section of steel and concrete was about three times larger compared to the steel section without concrete. Further, the concrete carried about 70% of the load, but the axial stress in the concrete, at an applied force of 150,000 lb, was less than 20% of the compressive strength of the concrete.

17. Document Analysis/Descriptors	18. Availability Statement
Composite construction, Reinforcing steel, Piles (Supports), Steel pipe, Axial loads, Bearing piles	No restrictions. Document available from: National Technical Information Services, Alexandria, Virginia 22312

19. Security Class (this report)	20. Security Class (this page)	21. No. of Pages	22. Price
Unclassified	Unclassified	39	

MECHANICAL RESPONSE OF A COMPOSITE STEEL, CONCRETE-FILLED PILE

FINAL REPORT

Prepared by:

Chen Hu
Jacob Sharpe
Joseph Labuz
Department of Civil, Environmental, and Geo- Engineering
University of Minnesota

June 2018

Published by:

Minnesota Department of Transportation
Research Services & Library
395 John Ireland Boulevard, MS 330
St. Paul, Minnesota 55155-1899

ACKNOWLEDGMENTS

The Technical Advisory Panel, Aaron Budge (Mn State Mankato), Derrick Dasenbrock (MnDOT),Thomas Johnson-Kaiser (MnDOT), Daniel Mattison (MnDOT), Jason Richter (MnDOT), and Andrew Shinnefield (MnDOT), provided valuable input at various stages of this project.

TABLE OF CONTENTS

LIST OF FIGURES

LIST OF TABLES

EXECUTIVE SUMMARY

The problem of load transfer within a composite pile composed of a steel-pipe section filled with concrete was investigated. For typical conditions (*e.g.,* Poisson's ratio of concrete $\nu^c < \nu^s$ of steel), the interaction between the steel pipe and concrete filling was shown to be negligible, which means that uniaxial stress conditions are a reasonable assumption to evaluate load on the composite pile. Experiments were conducted by applying axial load to an instrumented steel pipe-pile section (36 in. long, 12 in. ID, 0.25 in. wall thickness) filled with concrete (area of concrete $A^c \approx 12A^s$ of steel). Two types of strain gages, resistive and vibrating wire, were mounted to the steel pipe and measurements were validated by determining the known Young's modulus E^s of steel. Then, the steel-pipe section was filled with concrete and a resistive embedment gage was placed during the filling process to measure axial strain in the concrete. The axial load – axial strain responses of the steel and concrete were evaluated at various dates after placement. Concrete cylinders were cast at the same time that the concrete was placed in the pipe pile and the specimens were instrumented with resistive strain gages to measure axial and lateral strains. A curing effect, related to an increase in concrete stiffness, was studied by measuring Young's modulus E^c of the concrete cylinders on the same dates as load testing of the composite-pile section.

- Assuming the boundary condition of uniform axial displacement, *i.e.,* equal axial strain in the steel and concrete, $\varepsilon_z^s = \varepsilon_z^c = \varepsilon_z$, the sum of the forces carried by the two materials, $F^s + F^c$, where $F^s = \varepsilon_z * E^s * A^s$ and $F^c = \varepsilon_z * E^c * A^c$, provided a reasonable estimate – within 3% – of the pile force. Note that Young's modulus of the concrete must be known. Over a period of approximately 120 days, the Young's modulus of the concrete increased 5.5%.
- For the particular pile studied with a load condition of equal axial strains in the steel and concrete, the stiffness of the composite pile was about three times larger compared to the steel section without concrete. Further, the concrete carried about 70% of the load but the axial stress in the concrete, at an applied force of 150,000 lb, was less than 20% of the compressive strength of the concrete.
- If a load is applied to the steel pipe pile only but the bond between the steel and concrete is not broken, then the load is still carried by the steel section and the concrete filling, although the steel and concrete do not deform by the same amount. Because the axial strains in the steel and concrete are not equal, shear stress is generated along the steel-concrete interface and the shear stress "loads" the concrete. For the composite pile tested, the steel-concrete section is stiffer, about 2.7 times, compared to the steel pipe section with no concrete filling. Thus, the concrete is acting as more than a "filler," carrying about 60% of the load.

CHAPTER 1: INTRODUCTION

Load transfer is of key interest in geotechnical modeling and deep foundation performance. While load and deformation are relatively easy to measure in homogeneous concrete or steel members above-ground, subsurface composite sections passing through geologic strata exhibit various complexities. The goal of this study is to gain an improved understanding of load-deformation behavior of composite steel-concrete sections and examine phenomena related to shear stress along the steel-concrete interface and time-dependent stiffness effects, as well as the effectiveness of two types of sensors used to measure response.

MnDOT has several on-going research studies on pile foundations relating to load transfer, downdrag/dragload, and monitoring of pile performance. Several types of strain gages are being evaluated *in-situ,* and laboratory testing is needed to evaluate the performance of steel-concrete composite sections. This effort also ties into the MAP-21 framework for structural health monitoring and asset management.

In this project, a steel-pipe pile section, filled with concrete, was instrumented and tested. Two sensor types, resistive and vibrating wire strain gages, were mounted to the steel pipe and checked by determining the known elastic properties of steel. Then, the steel pipe was filled with concrete and an embedment gage was placed during the filling process. Load-strain response of the composite system was evaluated. The curing effects, related to an increase in Young's modulus of concrete, was also studied.

CHAPTER 2: PROCEDURES

A steel pipe pile section, approximately 3 ft long, was obtained from the field. Prior to the installation of strain gages, the steel pipe was placed in a metal lathe. The middle-third section of the steel pipe was cleaned to remove dirt and corrosion. The ends of the steel pipe were machined plane and perpendicular to the longitudinal axis.

Six resistive foil gages, three axial and three lateral, were bonded to the steel with a cyanoacrylate adhesive in the middle section and 120° apart. Lead wires were attached and a polyurethane waterproofing was applied. The mounting tabs for vibrating wire strain gages were welded directly to the steel pipe, 120° apart. Figure 2.1a shows the finished installation of the axial and lateral strain gages and Figure 2.1b shows the vibrating wire strain gage.

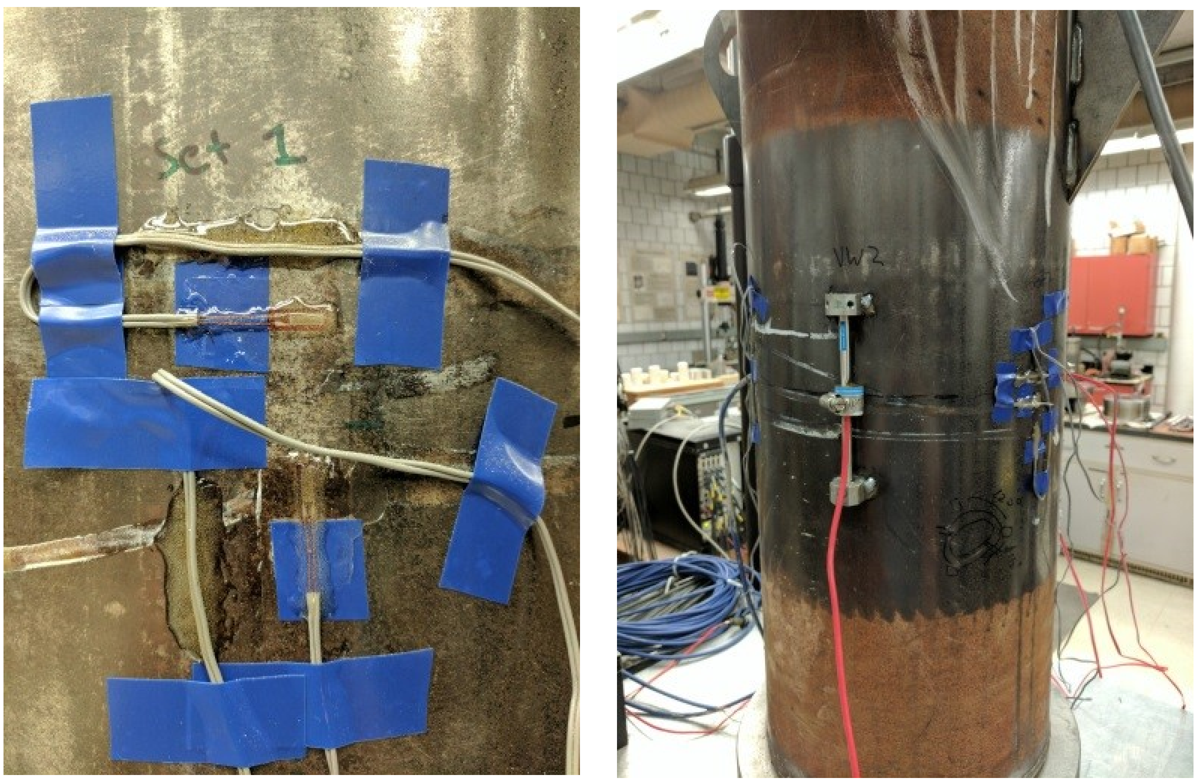

Figure 2.1 Photograph of strain gages on steel pipe. (a) Axial and lateral resistive strain gages. (b) Axial vibrating wire strain gage.

Before the pipe pile was filled with concrete, the instrumented section was placed in a 220,000 lb servo-hydraulic load frame and the response of the steel pipe was evaluated. Load and strains measured by the resistive and vibrating wire gages were digitally recorded at 1 Hz frequency.

After testing the steel section, the pipe pile was prepared to accommodate embedment gages: two axial embedment gages, one resistive (Tokyo Sokki Kenkyujo, PML-60) and one vibrating wire (Geokon Model 4200), and one lateral embedment gage (PML-60), were placed at the mid-height in the pipe prior to the placement of the concrete. The pipe assembly was filled with batch concrete (1x62CF, 5000 psi) to within 0.5 in. from the top of the pipe. Before filling the remaining 0.5 in. section of pipe with mortar, the composite pile was loaded by applying force to the steel pipe only. In addition, six 4 x 8 in. cylinders were cast from the batch concrete to evaluate the elastic parameters of the mix and changes with time (curing). Three cylinders were instrumented with axial and lateral resistive strain gages. Figure 2.2a shows a 4 x 8 in. concrete cylinder.

After approximately seven days, the 0.5 in. gap was filled with a high strength mortar (hydrostone) to ensure uniform contact between the steel loading plate and steel/concrete composite pile. Figure 2.2b shows the composite pile assembly placed in the testing machine. Load was transferred through a series of steel plates, starting with a 14 in. diameter steel plate (2 in. thickness), followed by 10- and 6-in. diameter steel plates (1 in. and 2 in. thick). Figure 2.2c shows the steel plate on top of the composite pile after the placing of hydrostone; holes in the steel plate allowed excess hydrostone to escape.

Testing was performed on June 8, 2017, seven (7) days after the concrete was mixed and poured (concrete cylinders were cast as well), on June 23, 2017, 21 days after mixing, and on October 23, 2017, 115 days after mixing; each test involved a load-unload cycle with strain readings. Young's modulus of the concrete was determined by uniaxial compression of the instrumented concrete cylinders. Table 2.1 shows the dates, experimental action, and concrete curing time.

Table 2.1 Procedures, dates, and concrete hardening time

Date	Action	Concrete Curing Time
May 22, 2017	Six strain gages were attached to the steel pipe. Pile section was loaded and strains were measured.	N/A
June 1, 2017	Steel pile was partially filled with concrete (0.5 in. gap). Concrete cylinders were cast.	0 days
June 7, 2017	Composite pipe pile was tested by loading the steel only. After the test, the 0.5 in gap was filled with mortar.	6 days
June 8, 2017	Composite pile and concrete cylinders were tested.	7 days
June 23, 2017	Composite pile and concrete cylinders were tested.	21 days
Oct 23, 2017	Composite pile and concrete cylinders were tested.	115 days

Figure 2.2 (a) Concrete cylinder with strain gages. (b) Composite pile within the load frame. (c) Steel plate on top of composite pile.

CHAPTER 3: ANALYSES

3.1 AXIAL DEFORMATION

A basic assumption of element testing is that the material deforms in a uniform manner. For example, a specimen that is originally cylindrical in shape remains a cylinder during testing. Ideally, the kinematic boundary condition imposed by a rigid platen means that the loading platen does not rotate but remains normal to the longitudinal axis of the specimen. However, some rotation is typically involved due to imperfections in specimen preparation and eccentricity in loading (Figure 3.1). Nonetheless, it is shown that the average of three deformation readings 120° apart provides the deformation due to the axial stress only.

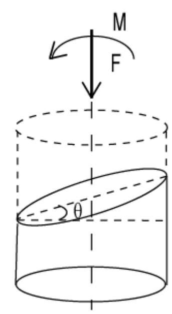

Figure 3.1 Axial force and moment imposed by rigid platens that rotate due to imperfections.

Consider the boundary condition imposed by a rigid platen that can rotate. The distribution of normal stress varies and the resultant is composed of an axial force and a bending moment. Thus, the total displacement can be decomposed into

$$\delta_{(i)} = \delta_{(i)F} + \delta_{(i)M} \tag{1}$$

where

$\delta_{(i)}$ = total displacement of i-sensor

$\delta_{(i)F}$ = displacement of i-sensor due to the axial force

$\delta_{(i)M}$ = displacement i-sensor due to the bending moment

Displacement due to the axial force (δ_F) will be the same for the three sensors. However, displacement due to the bending moment (δ_M) will depend on the angle of rotation (θ) and the position of the sensors relative to the axis of rotation. To describe the rotated plane, consider three sensors positioned at equi-angular positions, 120° apart. Because the axis of rotation is assumed to go through the center of the specimen, displacement of each sensor (*e.g.* LVDT) due to the bending moment will be decided by the position of the sensor in relation to the axis of rotation. If a sensor is on the axis of rotation, displacement due to bending moment is zero, and total displacement will be the same as axial displacement. If a sensor is located on a line perpendicular to the axis of rotation, displacement due to the bending moment will be either maximum δ_{max} or minimum δ_{min} (Figure 3.2).

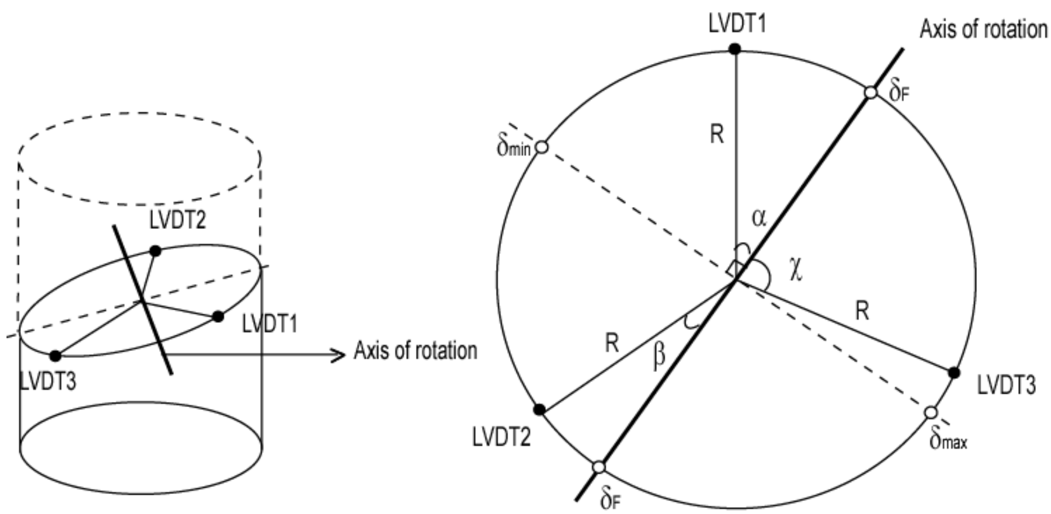

Figure 3.2 Geometry of specimen and sensors (LVDTs) with respect to the axis of rotation.

For a cylindrical specimen of radius R, define angles α, β, and χ as the angles between a line from the center of the specimen to each LVDT and the axis of rotation such that the location of δ_{min} is between LVDT1 and LVDT2. Therefore, the displacements of the three LVDTs are

$$\begin{aligned} \delta_1 &= \delta_F - R\,sin(\alpha)\,sin(\theta) \\ \delta_2 &= \delta_F - R\,sin(\beta)\,sin(\theta) \\ \delta_3 &= \delta_F + R\,sin(\chi)\,sin(\theta) \end{aligned} \tag{2}$$

and the sum is

$$\delta_1 + \delta_2 + \delta_3 = 3\delta_F - R\,sin(\theta)\,(sin(\alpha)+sin(\beta)-sin(\chi)) \tag{3}$$

For equi-angular placement of the three LVDTs, the last term becomes

$$sin(\alpha) + sin(\beta) - sin(\chi) = sin(\alpha) + sin(60°-\alpha) - sin(120°-\alpha) = 0 \tag{4}$$

From that:

$$\delta_F = (\delta_1 + \delta_2 + \delta_3)/3 = \delta_{average} \tag{5}$$

Consequently, the displacement due to axial force, even if rotation occurs, is simply the mean of the displacement values from the three sensors placed 120° apart. This means that rotation does not affect the value of the deformation for stiffness calculations.

3.2 COMPOSITE PILE INTERACTION

The axial load on a steel pipe pile filled with concrete can be calculated given the necessary strain measurements. The system is simplified as follows. The load is applied through a pile cap (steel plate), which is considered rigid. Displacement boundary conditions apply at the interface between the pile cap and the steel/concrete pile; this means that both the steel pipe and the concrete filling are assumed to have the same axial strain. The radial stress is the interaction pressure *p* between the steel pipe and the concrete due to Poisson's effect. Generalized Hooke's law in the axial direction is

$$\varepsilon_z = \frac{1}{E}\left(\sigma_z - 2\nu p\right) \tag{6}$$

So for the steel cylinder, with moduli E^s and ν^s, we can write

$$\sigma_z^s = E^s \varepsilon_z + 2\nu^s p \tag{7}$$

and for the concrete, with moduli E^c and ν^c, we can write

$$\sigma_z^c = E^c \varepsilon_z + 2\nu^c p \tag{8}$$

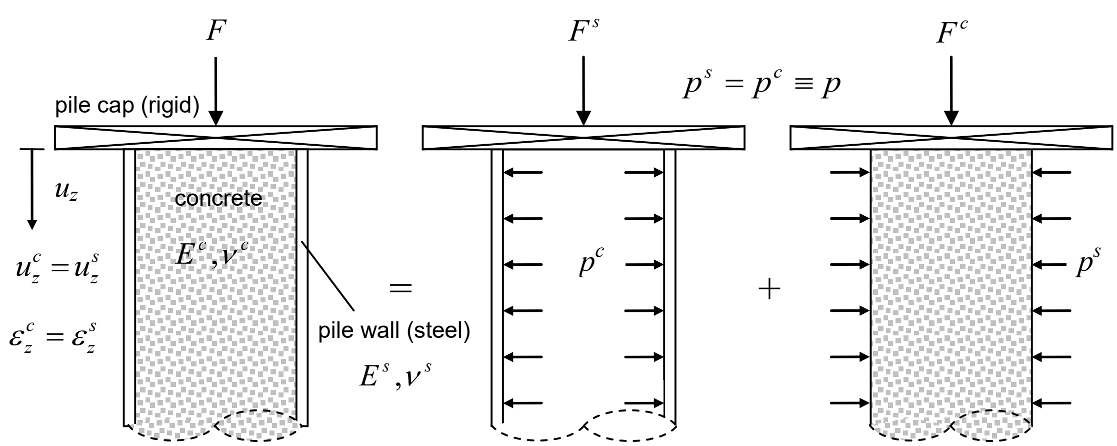

Figure 3.3 Sketch of the composite behavior of the steel-concrete pile.

For the thin-walled steel pipe, the radial displacement at *r* = *a* (outward displacement positive) is

$$u^s = \frac{a}{E^s}\left(p\,\frac{a}{b-a} + \nu^s \sigma_z^s\right) \tag{9}$$

For the solid concrete, the radial displacement at *r* = *a* is

$$u^c = \frac{a}{E^c}\left[-(1-\nu^c)p + \nu^c \sigma_z^c\right) \tag{10}$$

Substituting (7) and (8) into (9) and (10), we get

$$u^s = \frac{a}{E_s}[p\frac{a}{b-a} + \nu^s(E^s\varepsilon_z + 2\nu^s p)\,] \tag{11}$$

$$u^c = \frac{a}{E^c}\,[(1-\nu^c)p - \nu^c(E^c\varepsilon_z + 2\nu^c p)] \tag{12}$$

The interaction pressure p is determined from $u^s = u^c$:

$$\frac{1}{E^s}\left[p\frac{a}{b-a} + \nu^s(E^s\varepsilon_z + 2\nu^s p)\right] = \frac{1}{E^c}\,[-(1-\nu^c)p + \nu^c(E^c\varepsilon_z + 2\nu^c p)] \tag{13}$$

$$\Rightarrow\ \mathrm{p}\frac{a}{E^s\,(b-a)} + \nu^s\varepsilon_z + p\frac{2\nu^{s2}}{E^s} = \mathrm{p}\frac{-1+\nu^c}{E^c} + \nu^c\varepsilon_z + p\frac{2\nu^{c2}}{E^c} \tag{14}$$

$$\Rightarrow\ \varepsilon_z(\nu^c - \nu^s) = p\left[\frac{1}{E^c}\left(1-\nu^C - 2\nu^{c2}\right) + \frac{1}{E^s}\left(\frac{a}{b-a} + 2\nu^{s2}\right)\right] \tag{15}$$

$$p = \frac{\varepsilon_z\,(\nu^c - \nu^s)}{\frac{1}{E^c}\left(1-\nu^c-2\nu^{c2}\right)+\frac{1}{E^s}\left(\frac{a}{b-a}+2\nu^{s2}\right)} \tag{16}$$

Equation (16) allows the interaction pressure p to be computed from the measured strain ε_z, the known material parameters E and ν, and the geometry given by the inner (*a*) and outer (*b*) radii of the steel pipe. It is interesting to note that for typical concrete, $\nu^c < \nu^s$, so the interaction pressure is predicted to be negative – the concrete would be "pulling" on the steel. Perhaps some adhesion exists, but $p = 0$ is a reasonable approximation. Thus, with p taken to be negligible, only the axial strain in the steel or concrete must be measured (equations 7 and 8 with $p = 0$):

$$\sigma_z^s = E^s\varepsilon_z \tag{17}$$

$$\sigma_z^c = E^c\varepsilon_z \tag{18}$$

Once σ_z^s and σ_z^c are calculated, values for axial stress are multiplied by the respective cross-sectional areas and summed in order to obtain the total axial force:

$$\begin{aligned} F^{tot} &= F^s + F^c \\ &= \sigma_z^s A^s + \sigma_z^c A^c \end{aligned} \tag{19}$$

Force equilibrium applies no matter the loading, although when the kinematic boundary condition of constant displacement applies, the axial strain in the steel ε_z^s and concrete ε_z^c is the same so only one measurement of strain is required. If $\varepsilon_z^c \neq \varepsilon_z^s$ then shear stress develops at the steel-concrete interface and affects the force transmission; the total force is still the sum of two components, $F^s + F^c$, which must be calculated based on measurements of both ε_z^s and ε_z^c.

CHAPTER 4: RESULTS

4.1 STEEL PIPE PILE

Loading of the steel section without concrete was performed to evaluate the response of the strain gages, resistive and vibrating wire and to measure the elastic parameters of the steel. Figure 4.1 illustrates the positions of the strain gages. The plate welded to the bottom of the pipe contained a pin, which allowed precise placement of the assembly within the load frame. At the top of the pipe, the load transfer arrangement consisted of a steel plate that matched the diameter of the pipe (12.5 in.), along with three other plates, 14, 10, and 6 in. diameters.

Load and strain readings were recorded digitally while output from the vibrating wire gages was recorded manually. The results are shown in Figures 4.2 (resistive gages) and 4.3 (vibrating wire). The three strain readings show some nonuniformity in the deformation but the average strain value provides a reasonable estimate of Young's modulus E = 30,700 ksi (Figure 4.2). The vibrating wire gages require an adjustment to the gage factor, as the calculated E = 37,900 ksi is too large (Figure 4.3). For this reason, the vibrating wire gages were not used for further testing.

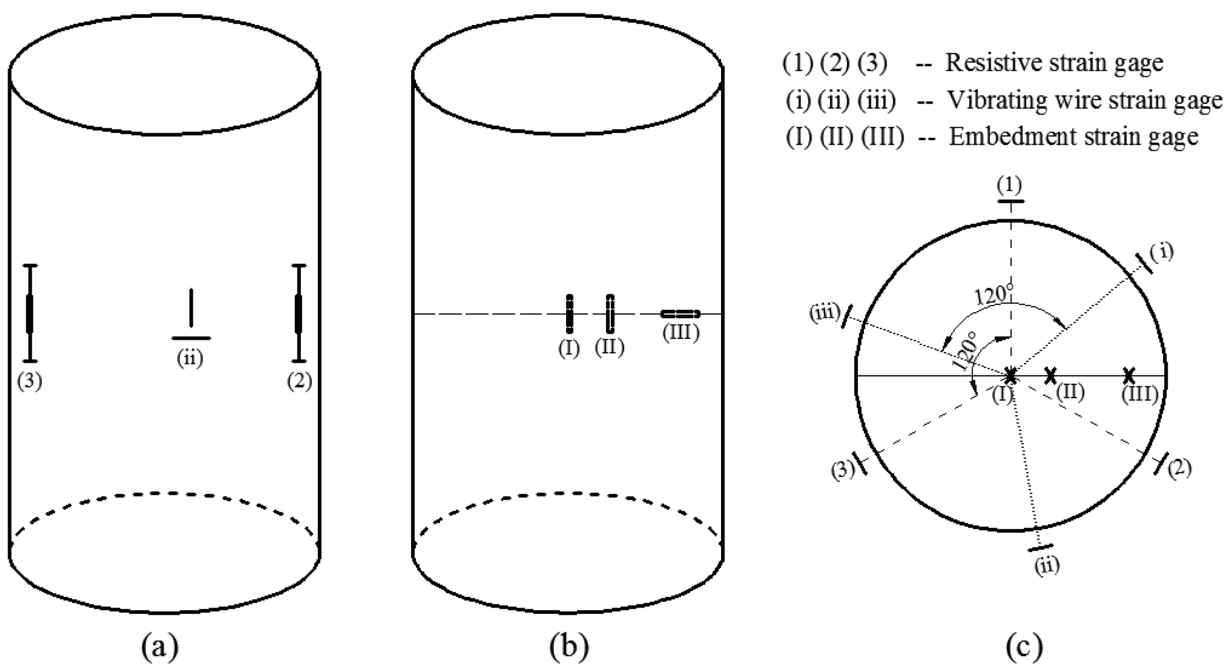

Figure 4.1 Strain gage numbers and their locations; (a) surface view; (b) inside view; (c) plan view.

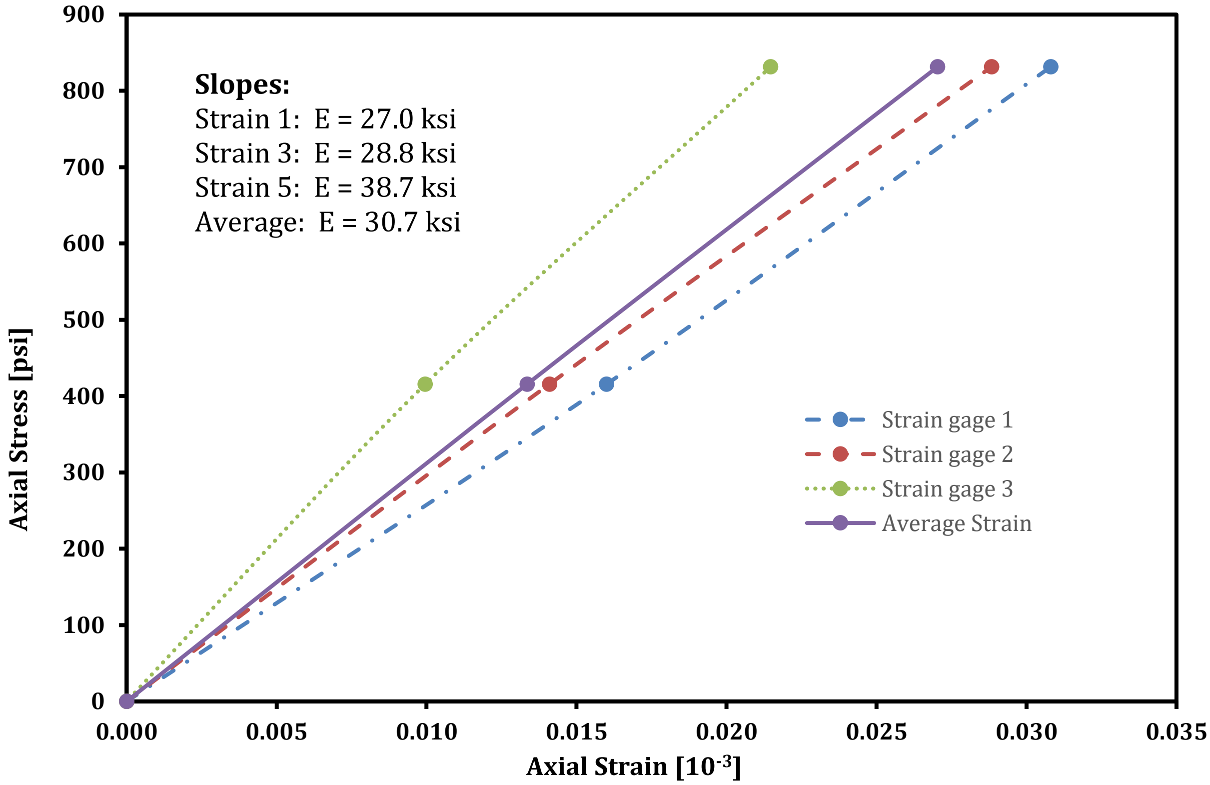

Figure 4.2 Stress-strain response of the steel pipe measured with resistive strain gages.

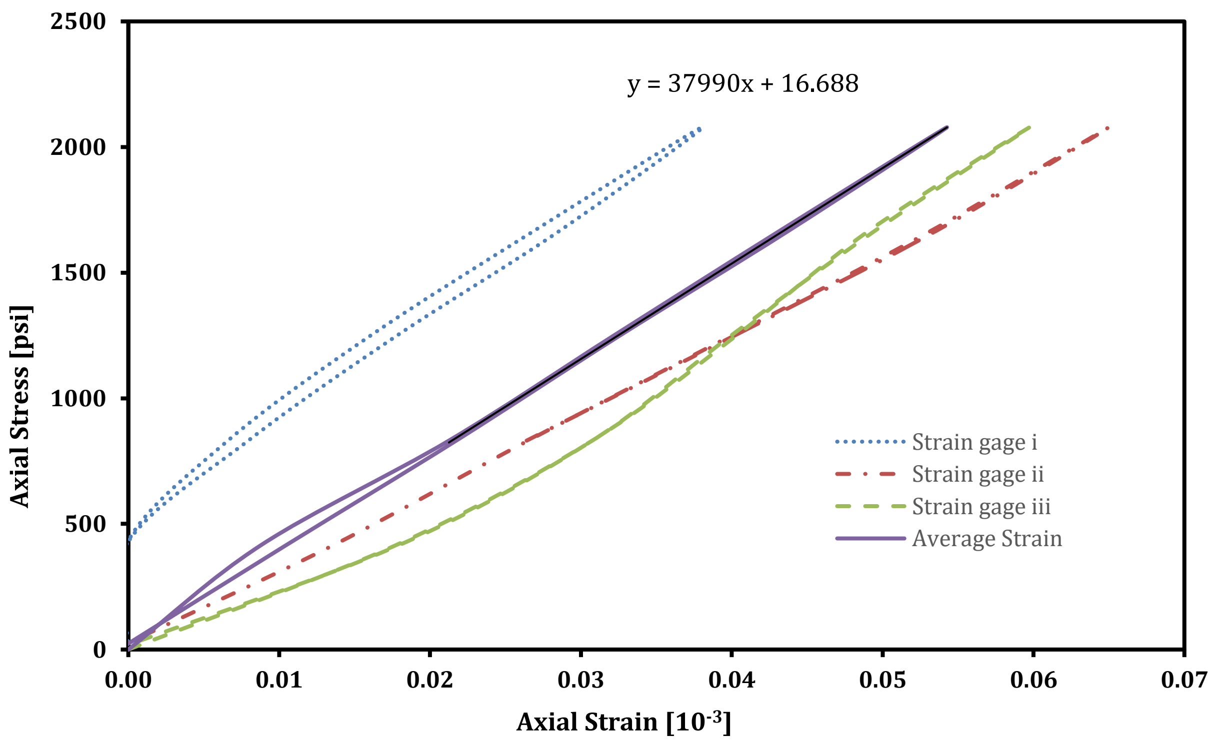

Figure 4.3 Stress-strain response of the steel pipe measured with vibrating wire strain gages.

4.2 PIPE PILE WITH CONCRETE, LOAD APPLIED TO STEEL

After concrete was placed in the steel pipe to within 0.5 in. of the top and allowed to cure for six days, the steel section of the composite pile was loaded to evaluate the mechanical behavior. The pile cap was in contact with the steel pipe but not the concrete filling, as shown in Figure 4.4. Thus, the applied force was only transferred to the steel but the response was affected by the concrete filling the pipe. Axial strains were measured using the concrete embedment (resistive) gage and the three (resistive) strain gages on the steel pipe. Relatively small values of axial load (< 20,000 lb) were applied to prevent damage at the steel-concrete interface. Figure 4.5 shows the response of the concrete embedment gage, where the very small values of strain (1×10^{-6}) were registered by the embedment gage. The oscillations were probably due to electrical noise.

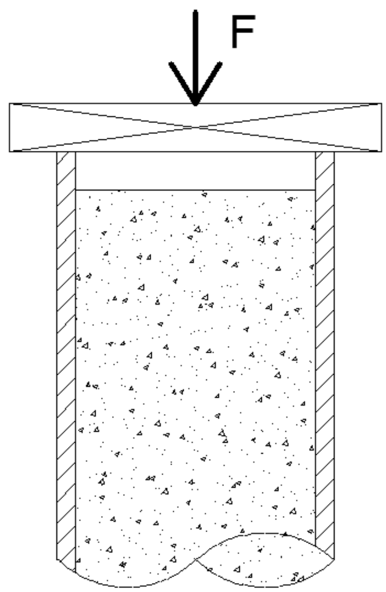

Figure 4.4 Sketch of the steel-concrete pile with loading applied to the steel only (no mortar).

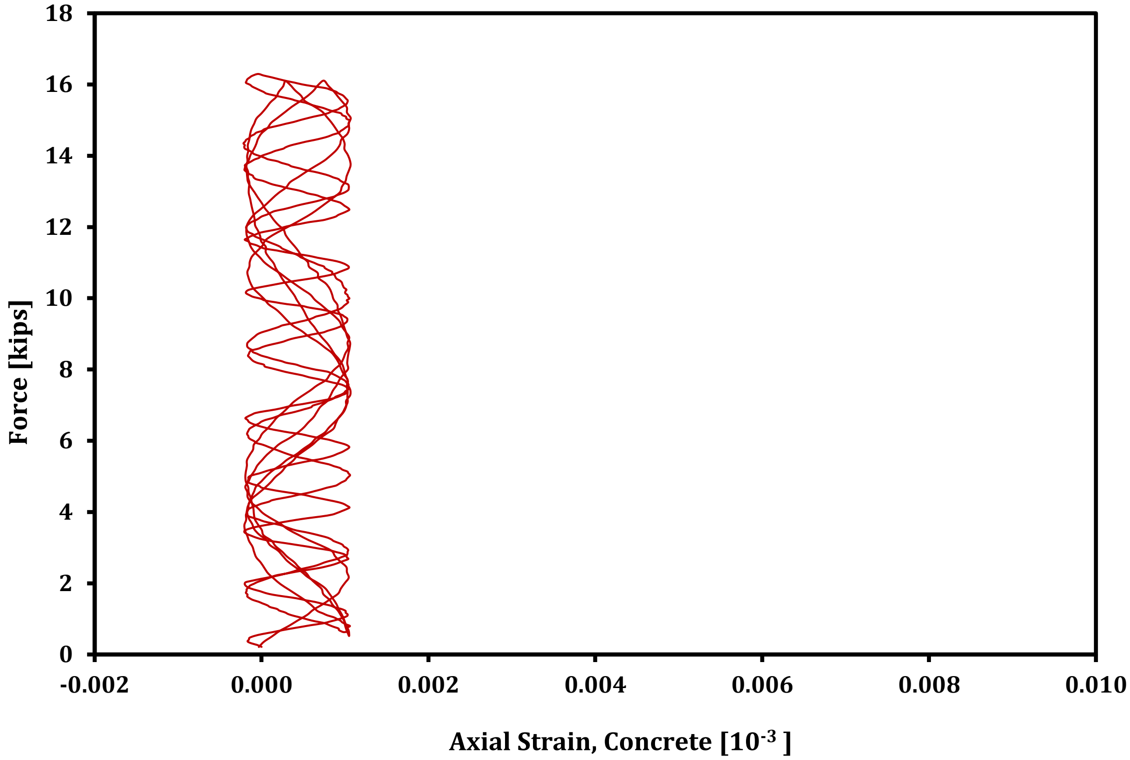

Figure 4.5 Force-strain response of the pipe measured with concrete strain gages.

Figure 4.6 shows the response of the composite pile, where the strain response, the average of the three (resistive) axial gages on the steel pipe, is linearized. The "calculated" force-strain curve is based on the uniaxial loading of an elastic (uniform) pipe, *i.e.* the concrete is not present, and confirmed by loading of the steel section (Figure 4.5). As illustrated in Figure 4.4, the load is applied to the steel section only; axial strain in the steel is different from the axial strain in the concrete and the result is the development of shear stress along the interface.

The difference between the two lines in Figure 4.6, at a particular value of strain, is the force in the concrete. The slope of the measured force-strain curve is $784*10^6$ lb while that of the calculated force-strain curve is $288*10^6$ lb. Even though the load is applied directly to the steel pipe, only 37% (288/784) is carried by the steel and 63% by the concrete, although the stress level in the concrete is well below its uniaxial strength. Thus, the concrete is acting as more than a "filler" and the stiffness [force/strain] of the composite pile is increased about 2.7 times, from $288*10^6$ lb to $784*10^6$ lb.

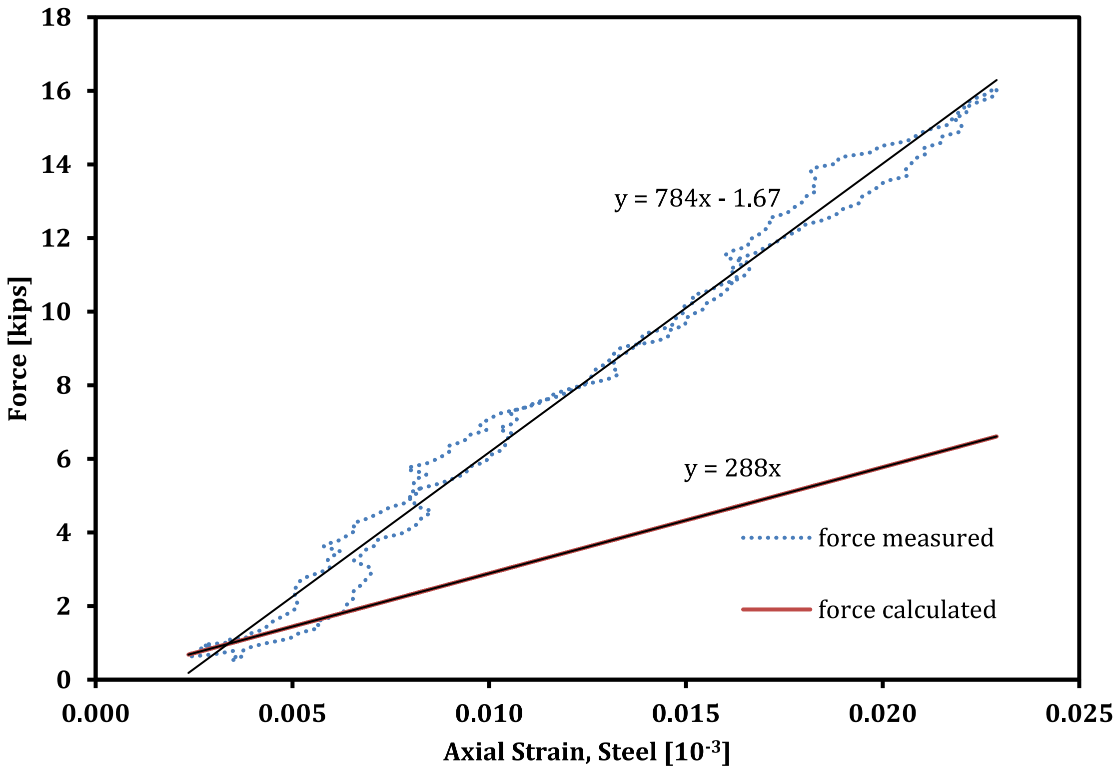

Figure 4.6 Force-strain response of the steel pipe section partially filled with concrete, (i) measured with resistive strain gages and (ii) calculated assuming a steel pipe only (no concrete filling).

Due to the difference in axial strain of the steel pipe and concrete filling, shear stress is generated along the interface. Figure 4.7 is a schematic representation of the condition where load was only applied to the steel pile. Because shear stress acts opposite to the displacement, during the loading process, shear stress acted downward on the concrete and upward on the steel. During an unloading process, the shear stress would change its direction.

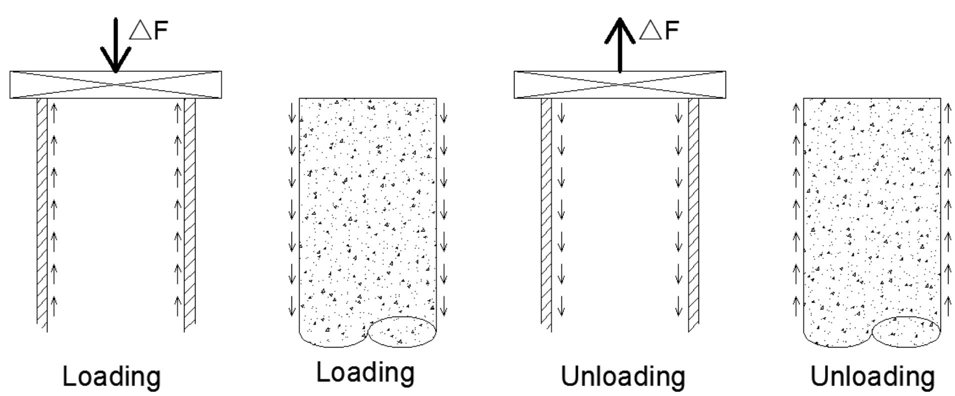

Figure 4.7 Sketch of the composite behavior of the steel-concrete pile when loading the steel; shear stress develops along the interface.

The effect is similar if loading is only applied to the concrete in that shear stress develops along the interface, as shown in Figure 4.8. Compared to the "steel-only" scenario, the shear stress would act upward on the concrete and act downward on the steel in the loading process, and act downward on the concrete and act upward on the steel in the unloading process.

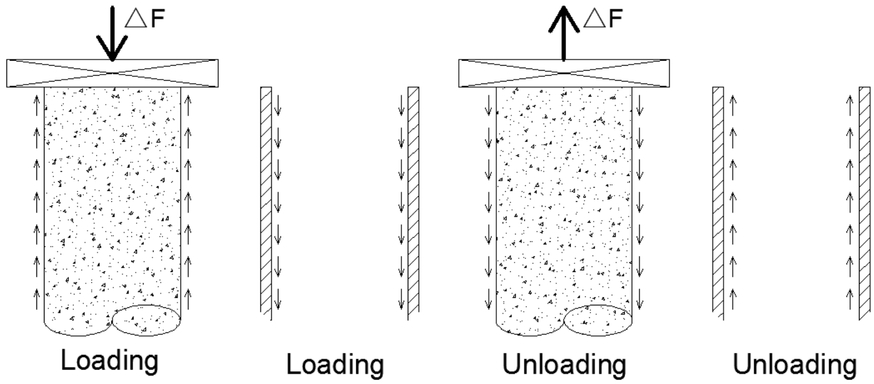

Figure 4.8 Sketch of the composite behavior of the steel-concrete pile when loading the concrete only.

4.3 PIPE PILE WITH CONCRETE, LOAD APPLIED TO BOTH

The composite behavior of the pipe pile filled with concrete was investigated by imposing the same displacement to the steel and the concrete and measuring the force. Recall that the 0.5 in. gap was filled with mortar and a steel plate rested on both the steel and mortar (concrete). The load arrangement of constant displacement – the same axial strain in the steel and concrete – was anticipated. Three resistive axial strain gages mounted to the steel and one resistive embedment gage placed within the concrete were connected to the data acquisition system. Three load cycles were applied: two up to a maximum load of 100,000 lb and one to 120,000 lb (Figures 4.9, 4.10, and 4.11). Ideally, if the steel and the concrete deformed the same amount axially, the force – axial strain response, *i.e.* the slopes k^s for the steel and k^c for the concrete, would be identical. (Note that the accuracy of the resistive embedment gage was not assessed.)

For the June 8 test, the average stiffnesses (force/unit strain or simply force) were $k^s = 900*10^6$ lb ($889.9*10^6$, $899.3*10^6$, $908.0*10^6$ lb) from the "steel" strain and $k^c = 890*10^6$ lb ($887.0*10^6$, $882.7*10^6$, $901.5*10^6$ lb) from the "concrete" strain. Taking the response of the composite section to be well described by the resistive strain gages on the steel, $k^s = k^c = k = 900*10^6$ lb, the pipe pile with concrete is about three times stiffer than the steel section with no concrete (900/290 = 3.1).

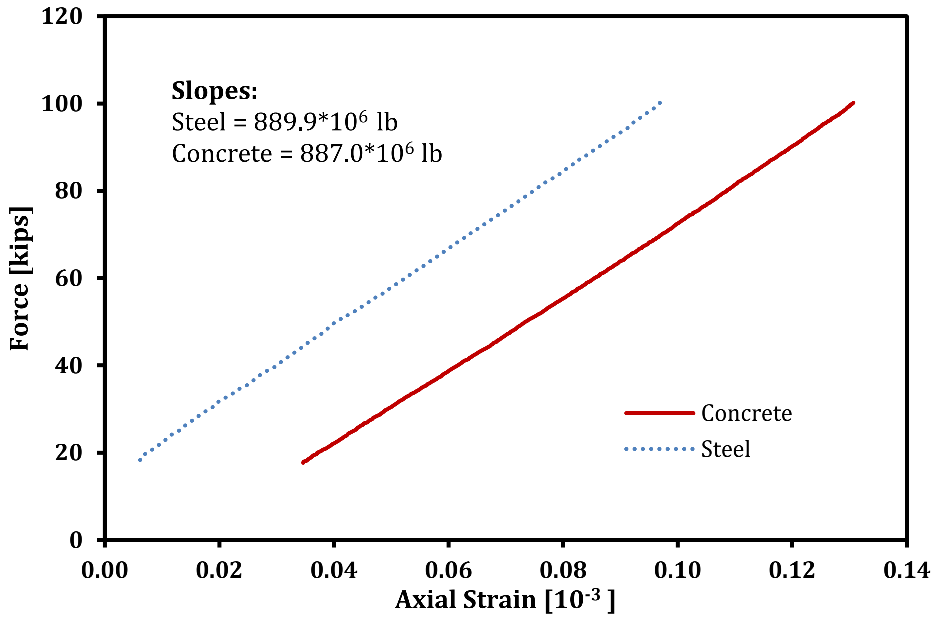

Figure 4.9 Load cycle 1. The steel response is the average of the three resistive gages; the concrete response is from the resistive embedment gage.

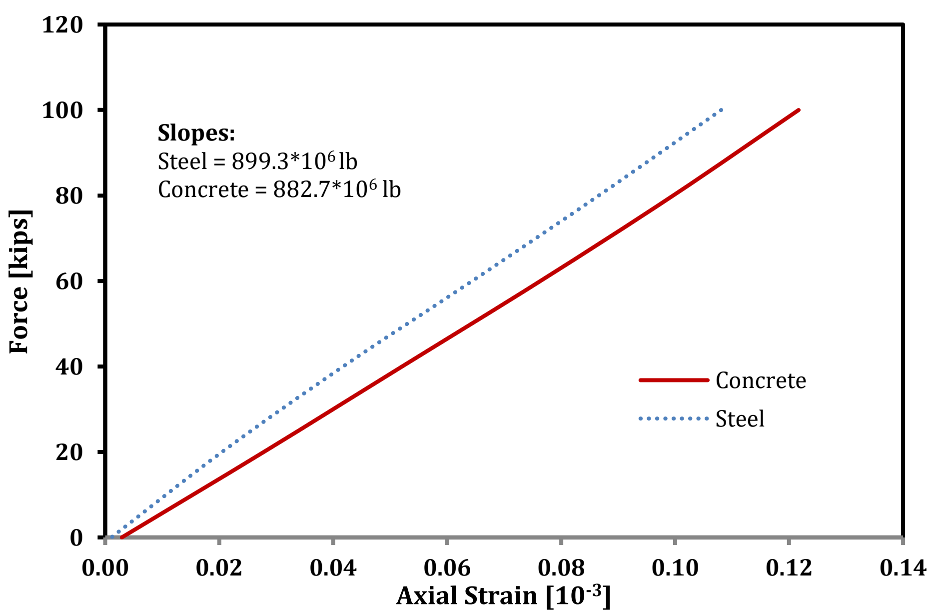

Figure 4.10 Load cycle 2. The steel response is the average of the three resistive gages; the concrete response is from the resistive embedment gage.

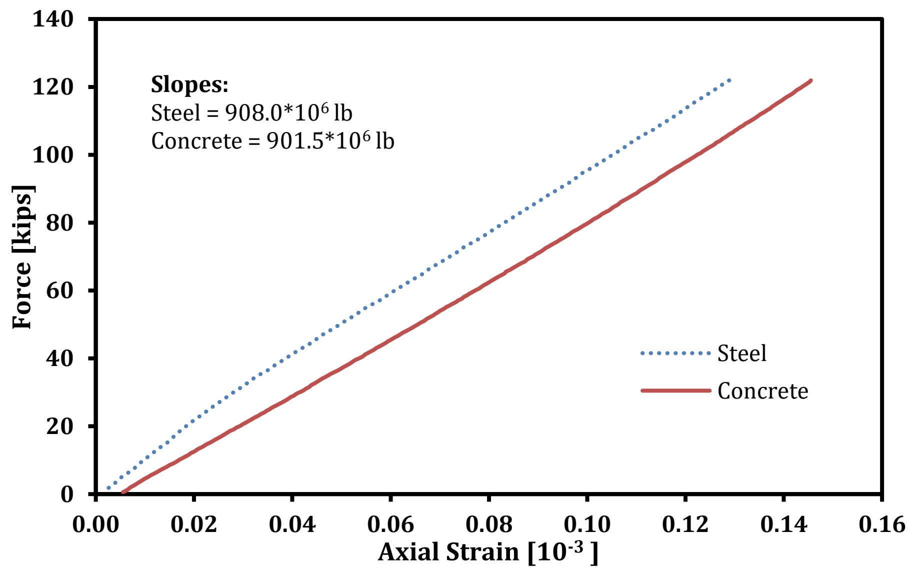

Figure 4.11 Load cycle 3. The steel response is the average of the three resistive gages; the concrete response is from the resistive embedment gage.

Even with the unknown accuracy of the concrete embedment gage, it appears that assumption of the same axial strain in the steel and concrete is reasonable. Two cases are considered: (i) axial strains are equal and represented by k^s, where ε_z = F_appl / k^s; (ii) axial strains are equal and represented by k^c, where ε_z = F_appl / k^c. F_calc is based on the force in each material computed from the axial strain, where F_calc = F_s + F_c, F_s = ε_z^s * E^s * A^s, and F_c = ε_z^c * E^c * A^c. Young's modulus of steel E^s = 30,000 ksi and Young's modulus of concrete E^c = 5,500 ksi.

Case (i): axial strains are equal and represented by k^s, where ε_z = F_appl / k^s. Table 4.1 shows the comparison of applied force versus calculated force, with interaction pressure taken as zero (p = 0). The calculated force is within 1.2%, assuming that the axial strains ε_z in the steel and concrete are equal and determined from k^s.

Table 4.1 Force calculation based on k^s = 900*10⁶ lb from June 8 test and $\varepsilon_z^c = \varepsilon_z^s$.

Es	nu_s	Ec	nu_c	a	b	As	Ac
psi	[-]	psi	[-]	in.	in.	in.^{2}	in.^{2}
30000000	0.26	5500000	0.19	6.00	6.25	9.62	113.10
F_appl	ε	σ_s	σ_c	F_s	F_c	F_calc	difference
kips	10^{-6}	psi	psi	lb	lb	kips	%
10.0	11	333	61	3207	6912	10.12	1.18
20.0	22	667	122	6413	13823	20.24	1.18
30.0	33	1000	183	9620	20735	30.36	1.18
40.0	44	1333	244	12827	27647	40.47	1.18
50.0	56	1667	306	16033	34558	50.59	1.18

F_appl	ε	σ_s	σ_c	F_s	F_c	F_calc	difference
60.0	67	2000	367	19240	41470	60.71	1.18
70.0	78	2333	428	22447	48382	70.83	1.18
80.0	89	2667	489	25653	55293	80.95	1.18
90.0	100	3000	550	28860	62205	91.07	1.18
100.0	111	3333	611	32067	69117	101.18	1.18
110.0	122	3667	672	35273	76028	111.30	1.18
120.0	133	4000	733	38480	82940	121.42	1.18
130.0	144	4333	794	41687	89852	131.54	1.18
150.0	167	5000	917	48100	103675	151.78	1.18

Case (ii): axial strains are equal and represented by k^c, where ε_z = F_appl / k^c. Table 4.2 shows the comparison of applied force versus calculated force, with interaction pressure taken as zero (p = 0). The calculated force is within 2.3%, assuming that the axial strains ε_z in the steel and concrete are equal and determined from k^c.

Table 4.2 Force calculation based on $k^c = 890*10^6$ lb from June 8 test and $\varepsilon_z^c = \varepsilon_z^s$.

Es	nu_s	Ec	nu_c	a	b	As	Ac
psi	[-]	psi	[-]	in.	in.	in.^{2}	in.^{2}
30000000	0.26	5500000	0.19	6.00	6.25	9.62	113.10
F_measued	ε	σ_s	σ_c	F_s	F_c	F_calc	difference
kips	10^{-6}	psi	psi	lb	lb	kips	%
10.0	11	337	62	3243	6989	10.23	2.32
20.0	22	674	124	6485	13979	20.46	2.32
30.0	34	1011	185	9728	20968	30.70	2.32
40.0	45	1348	247	12971	27957	40.93	2.32
50.0	56	1685	309	16213	34947	51.16	2.32
60.0	67	2022	371	19456	41936	61.39	2.32
70.0	79	2360	433	22699	48925	71.62	2.32
80.0	90	2697	494	25942	55915	81.86	2.32
90.0	101	3034	556	29184	62904	92.09	2.32
100.0	112	3371	618	32427	69893	102.32	2.32
110.0	124	3708	680	35670	76883	112.55	2.32
120.0	135	4045	742	38912	83872	122.78	2.32
130.0	146	4382	803	42155	90861	133.02	2.32
150.0	169	5056	927	48640	104840	153.48	2.32

4.4 PIPE PILE WITH CONCRETE, CURING EFFECT

Young's modulus of the concrete can increase with time because of the curing process and an increase in E^c will increase the stiffness of the system. Two other tests were performed, one on June 23, 2017 (21 days after placement) and one on October 23, 2017 (115 days after placement). The corresponding concrete modulus was determined by loading the concrete cylinders and measuring axial strain. Young's modulus of the concrete E^c increased 2.5% and 5.5% after 21 and 115 days: E^c = 5,550 ksi at seven days, 5,640 ksi at 21 days (Figure 4.12), and 5,750 ksi at 115 days (Figure 4.14). The total stiffness of the composite pile, as measured by the axial strain in the concrete, also increased from approximately $900*10^6$ lb to $930*10^6$ lb (Figure 4.13) to $970*10^6$ lb (Figure 4.15). Based on the October 23 test, the calculated load was 146,400 lb and the applied load was 150,000 lb, a percent difference of 2.4%. Figure 4.16 shows the increase in Young's modulus and pile stiffness as the concrete cured.

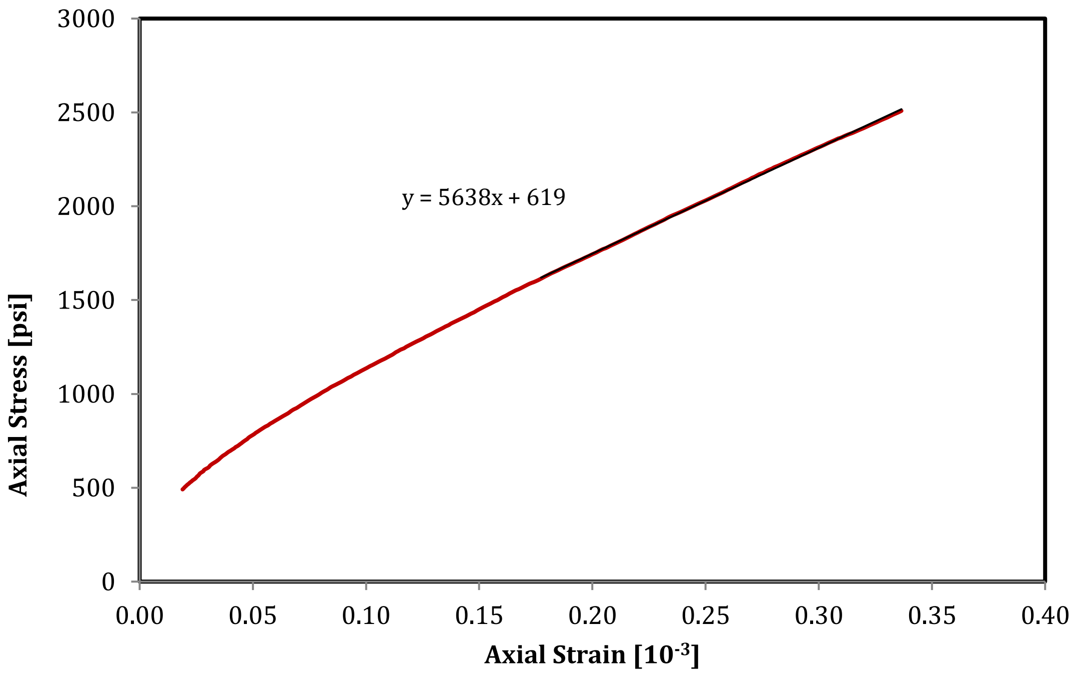

Figure 4.12 Concrete cylinder stress-strain response on June 23, 21 days after mixing.

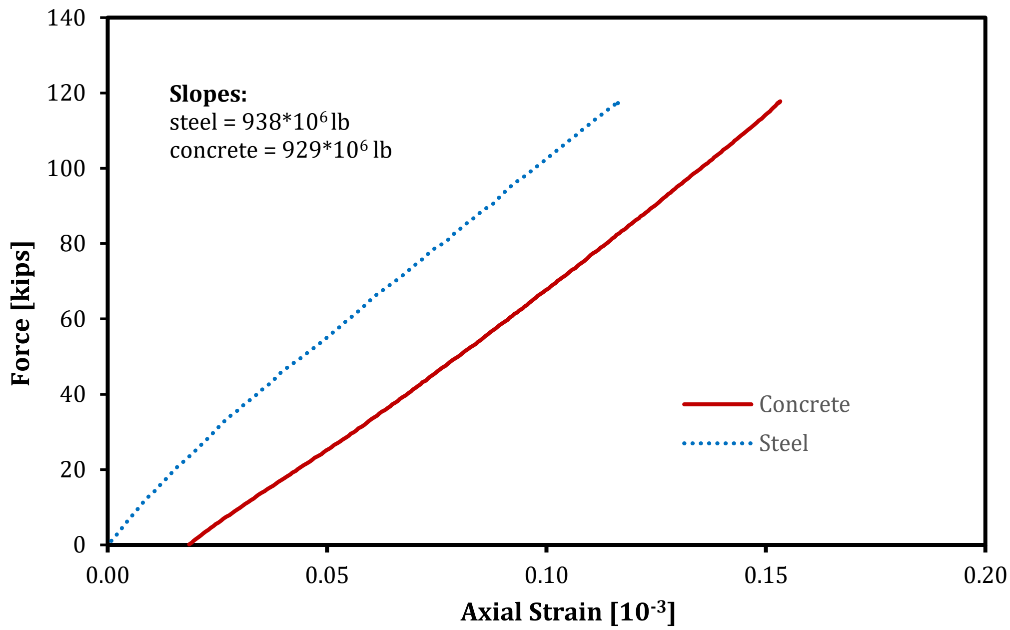

Figure 4.13 composite pile force-strain response on June 23, 21 days after mixing.

Table 4.3 Force calculation based on k^c = 953*10^6 lb from June 23 test and $\varepsilon_z^c = \varepsilon_z^s$.

Es	nu_s	Ec	nu_c	a	b	As	Ac
psi	[-]	psi	[-]	in.	in.	in.^{2}	in.^{2}
30000000	0.26	5640000	0.19	6.00	6.25	9.62	113.10
F_appl	ε	σ_s	σ_c	F_s	F_c	F_calc	difference
kips	10^{-6}	psi	psi	lb	lb	kips	%
10.0	11	323	61	3107	6866	9.97	0.27
20.0	22	646	121	6213	13733	19.95	0.27
30.0	32	969	182	9320	20599	29.92	0.27
40.0	43	1292	243	12426	27465	39.89	0.27
50.0	54	1615	304	15533	34332	49.86	0.27
60.0	65	1938	364	18639	41198	59.84	0.27
70.0	75	2260	425	21746	48064	69.81	0.27
80.0	86	2583	486	24853	54931	79.78	0.27
90.0	97	2906	546	27959	61797	89.76	0.27
100.0	108	3229	607	31066	68664	99.73	0.27
110.0	118	3552	668	34172	75530	109.70	0.27
120.0	129	3875	729	37279	82396	119.68	0.27
130.0	140	4198	789	40385	89263	129.65	0.27
150.0	161	4844	911	46598	102995	149.59	0.27

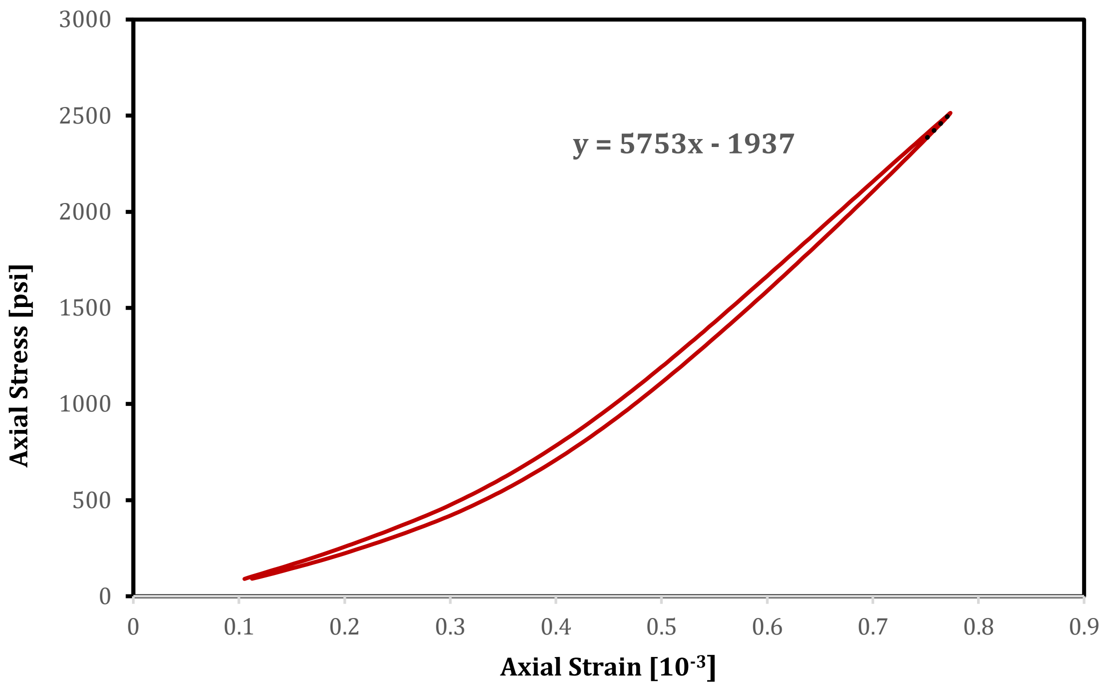

Figure 4.14 Concrete cylinder stress-strain response on October 23, 115 days after mixing.

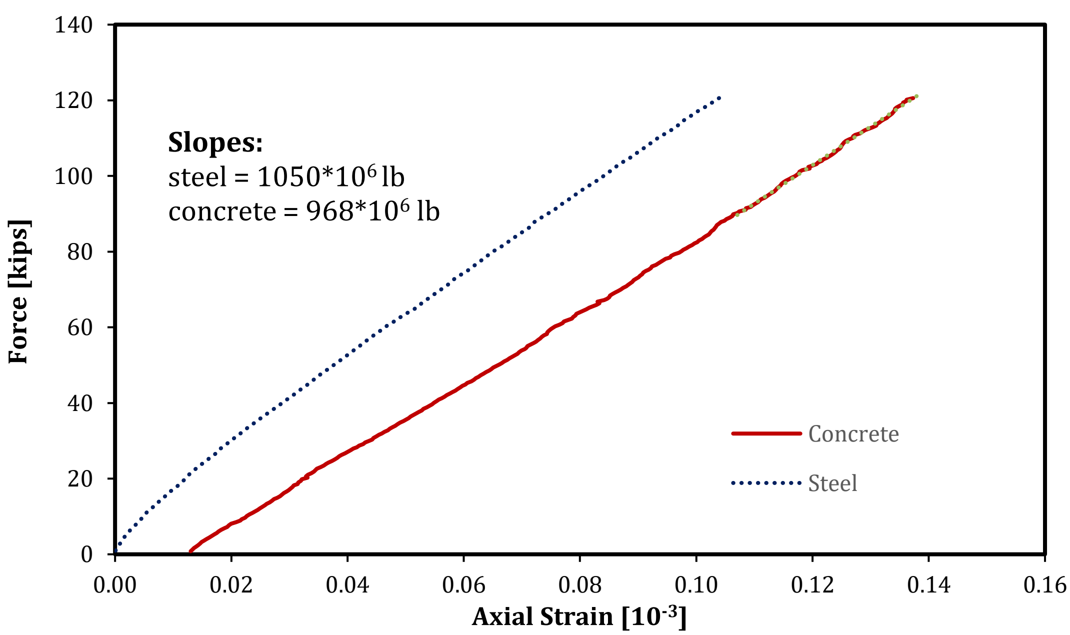

Figure 4.15 Composite pile force-strain response on October 23, 115 days after mixing.

Table 4.4 Force calculation based on $k^c = 968*10^6$ lb from October 23 test and $\varepsilon_z^c = \varepsilon_z^s$.

Es	nu	Ec	nu	a	b	As	Ac
psi	[-]	psi	[-]	in.	in.	in.^{2}	in.^{2}
30000000	0.26	5800000	0.19	6.00	6.25	9.62	113.10
F_appl	ε	σ_s	σ_c	F_s	F_c	F_calc	difference
kips	10^{-6}	psi	psi	lb	lb	kips	%
10.0	10	310	60	2981	6777	9.76	2.42
20.0	21	620	120	5963	13553	19.52	2.42
30.0	31	930	180	8944	20330	29.27	2.42
40.0	41	1240	240	11926	27107	39.03	2.42
50.0	52	1550	300	14907	33883	48.79	2.42
60.0	62	1860	360	17888	40660	58.55	2.42
70.0	72	2169	419	20870	47437	68.31	2.42
80.0	83	2479	479	23851	54213	78.06	2.42
90.0	93	2789	539	26833	60990	87.82	2.42
100.0	103	3099	599	29814	67767	97.58	2.42
110.0	114	3409	659	32795	74543	107.34	2.42
120.0	124	3719	719	35777	81320	117.10	2.42
130.0	134	4029	779	38758	88096	126.85	2.42
150.0	155	4649	899	44721	101650	146.37	2.42

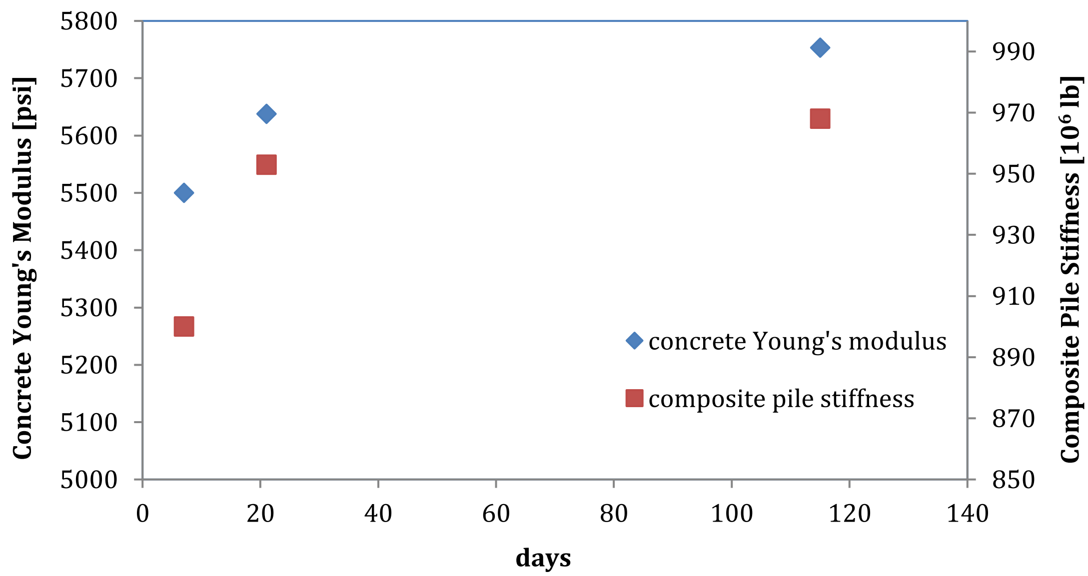

Figure 4.16 Increase of concrete Young’s modulus and composite pile stiffness with time.

CHAPTER 5: CONCLUSIONS

The problem of load transfer within a composite pile composed of a steel-pipe section filled with concrete was investigated. For typical conditions – thin-walled steel pipe, concrete area A^c an order of magnitude larger than steel area A^s, and Poisson's ratio of concrete $\nu^c < \nu^s$ of steel – the interaction between the steel pipe and concrete filling is negligible and uniaxial stress conditions are a reasonable assumption to evaluate the force on the composite pile. Therefore, if the steel pipe and concrete filling deform the same, then the applied force can be determined by measuring the strain in one material (*e.g.* concrete) and knowing Young's modulus of both steel E^s and concrete E^c.

Experiments were conducted by applying axial load to an instrumented steel pipe-pile section (12 in. ID, 0.25 in. wall thickness) filled with concrete (area of concrete $A^c \approx 12A^s$ of steel). Two types of strain gages, resistive and vibrating wire, were mounted to the steel pipe and measurements were validated by determining the known elastic properties of the steel. The steel-pipe section was filled with concrete, and a resistive embedment gage was placed during the filling process to measure axial strain in the concrete. The axial load – axial strain responses of the steel and concrete were evaluated at various dates after placement. Concrete cylinders were cast at the same time that the concrete was placed in the pipe pile and the specimens were instrumented with resistive strain gages to measure axial strains. The effect related to concrete curing was studied by measuring Young's modulus of the concrete cylinders on the same dates as load testing of the composite-pile section.

Assuming the boundary condition of uniform axial displacement, *i.e.,* equal axial strain in the steel and concrete, $\varepsilon_z^s = \varepsilon_z^c = \varepsilon_z$, the sum of the forces carried by the two materials, $F^s + F^c$, where $F^s = \varepsilon_z * E^s * A^s$ and $F^c = \varepsilon_z * E^c * A^c$, provided a reasonable estimate – within 3% – of the pile force as long as Young's modulus of the concrete was known. As the concrete cured, Young's modulus increased; *e.g.,* after curing for about 120 days, the modulus increased 5.5%. If this effect was not considered, the load on the pile would be under-estimated.

For the particular section evaluated (area of steel A^s = 9.62 in.^{2} and area of concrete A^c = 113.10 in.^{2}), if the load is applied to both the steel and the concrete such that the axial strains are approximately equal, then the stiffness of the composite pile is about three times larger compared to the steel section without concrete. Further, the concrete carries about 70% of the load but the axial stress in the concrete, at an applied force of 150,000 lb, is less than 20% of the compressive strength of the concrete.

APPENDIX A: FORCE – AXIAL STRAIN PLOTS

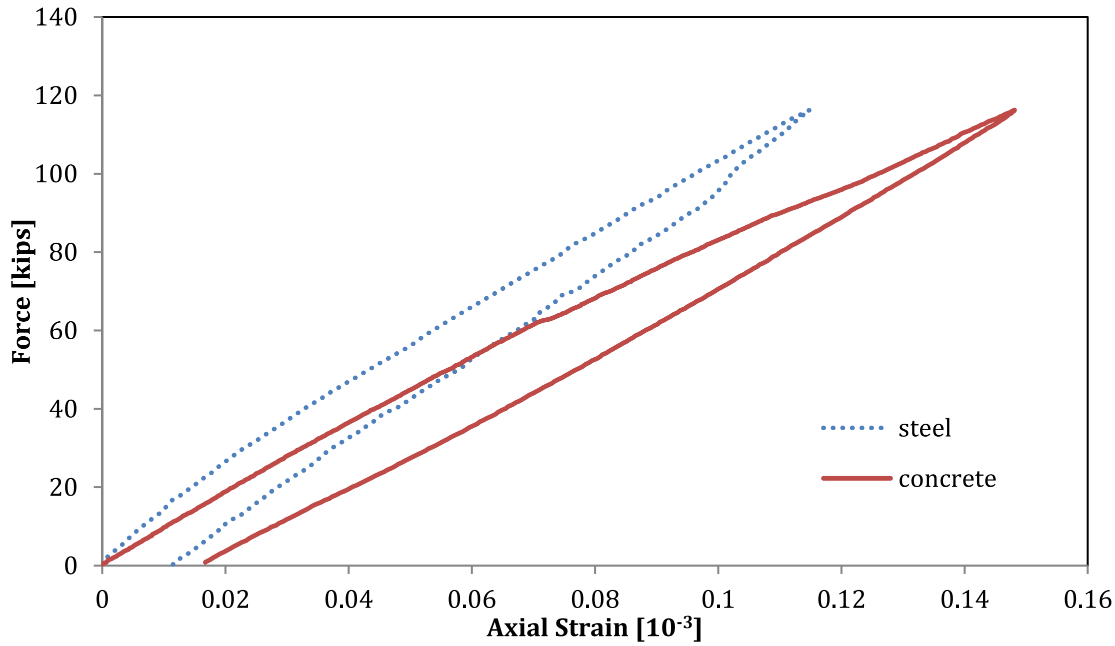

Figure A.1 Load cycle one for June 23 test.

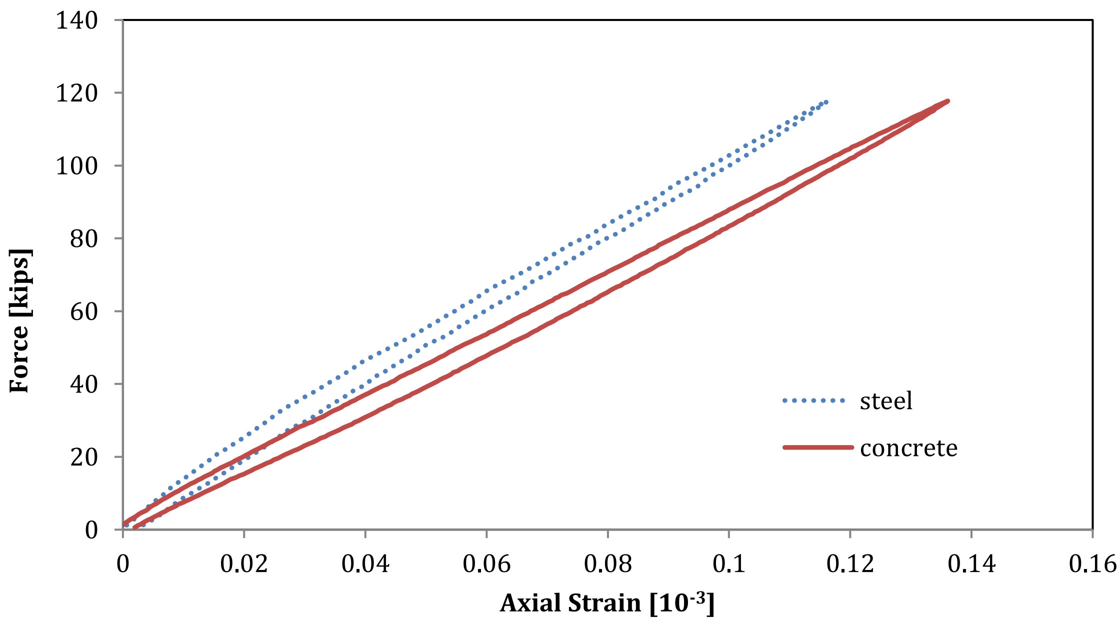

Figure A.2 Load cycle two for June 23 test.

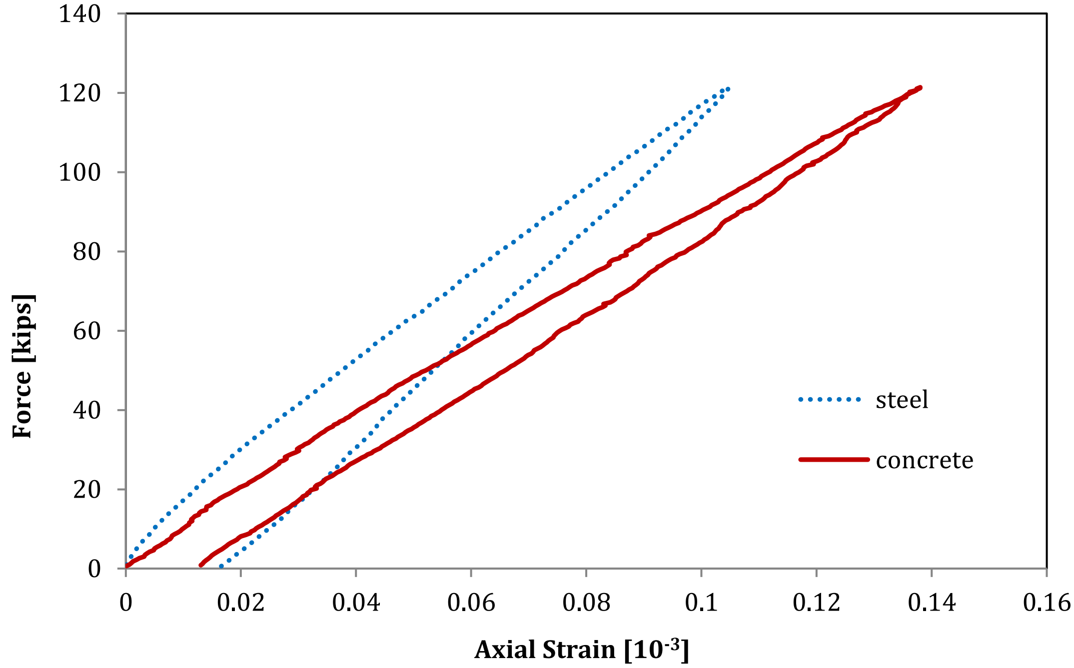

Figure A.3 Load cycle one for October 23 test.

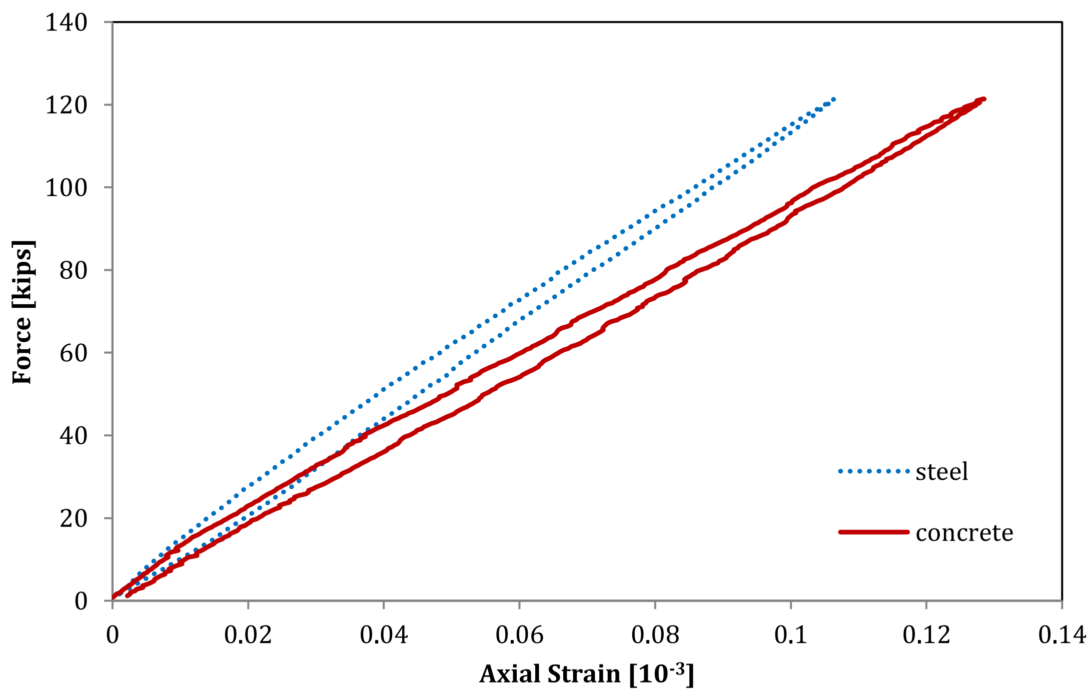

Figure A.4 Load cycle two for October 23 test.

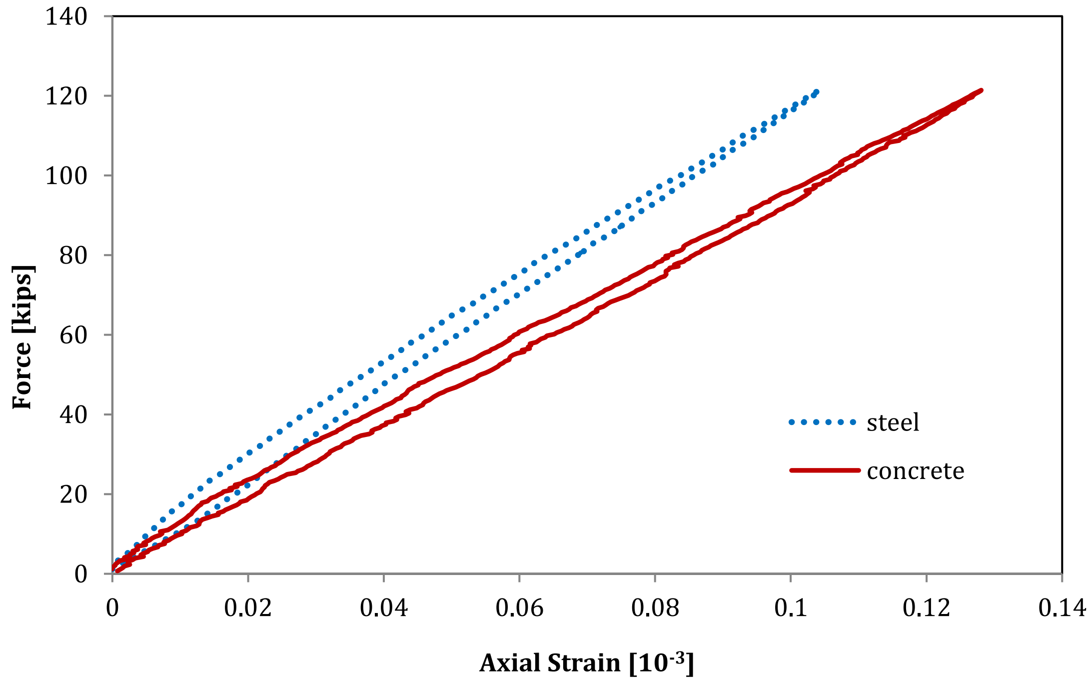

Figure A.5 Load cycle three for October 23 test.

APPENDIX B: PHOTOS

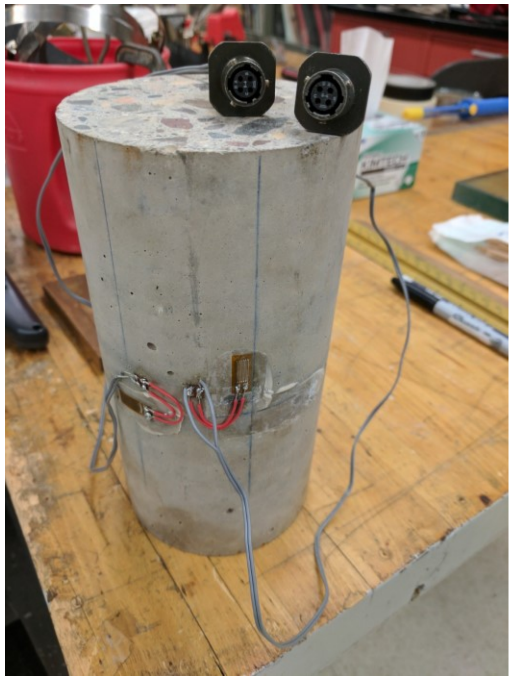

Figure B.1 Concrete cylinder with strain gages

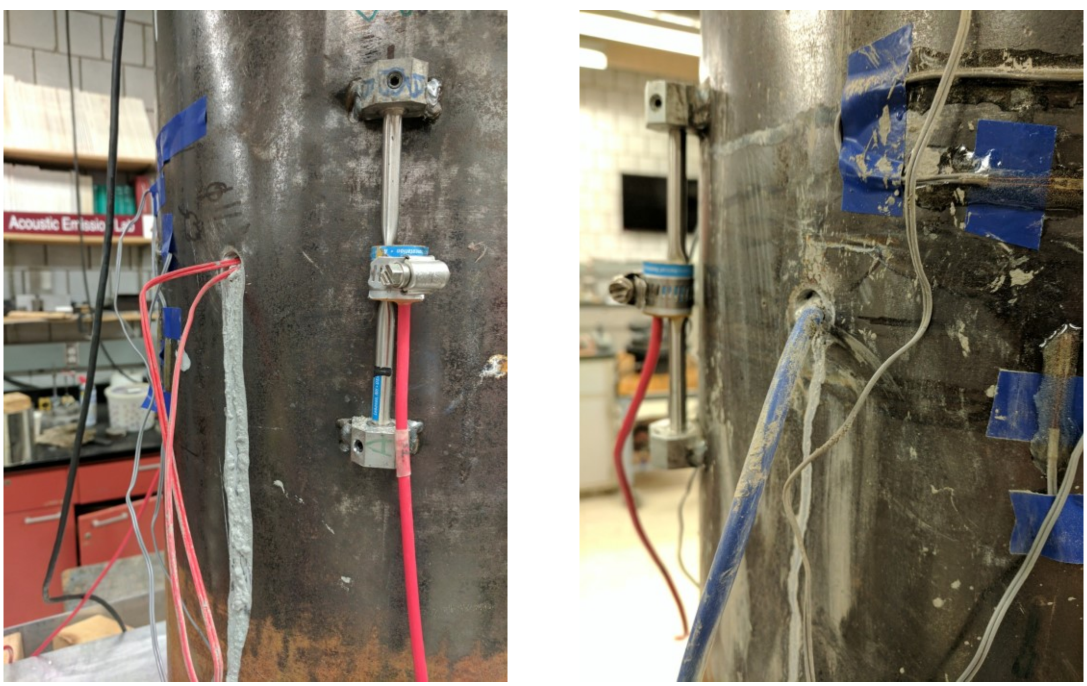

Figure B.2 (a) Vibrating wire strain gage. (b) Embedment hole on steel pile

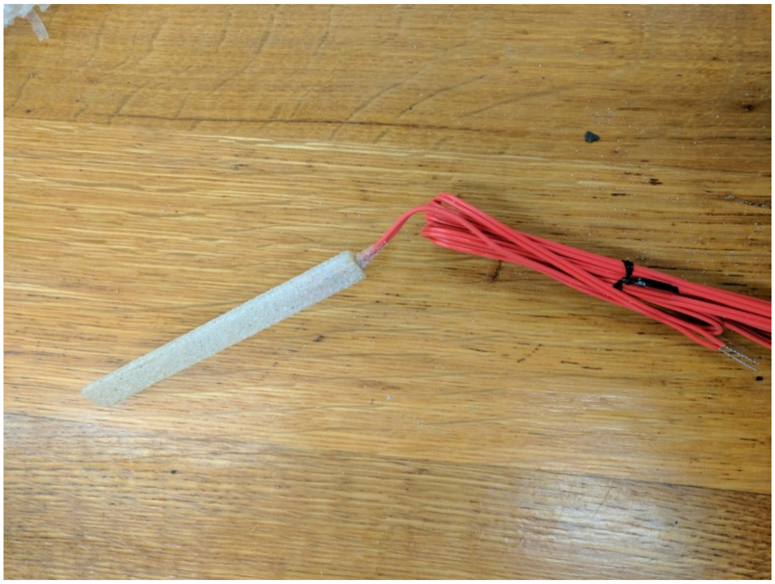

Figure B.3 Embedment resistive strain gage

Figure B.4 Steel pipe before machining.

Figure B.5 Vibrating wire strain gage on pile surface